ANL-90/20

Fixed Mask Assembly Research for APS Insertion Devices

by Tuncer M. Kuzay

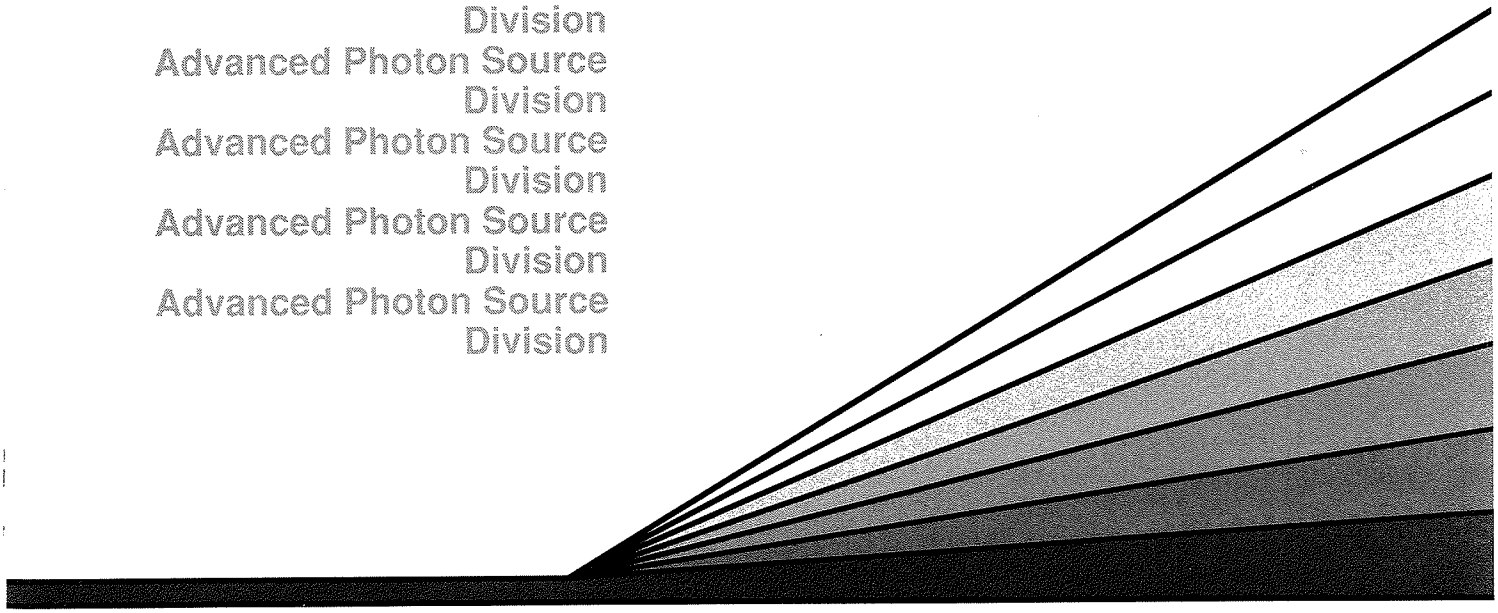

Argonne National Laboratory, Argonne, Illinois 60439
operated by The University of Chicago
for the United States Department of Energy under Contract W-31-109-Eng-38

This report has been reproduced from the best available copy.

Available from the
National Technical Information Service
U.S. Department of Commerce
5285 Port Royal Road
Springfield, VA 22161

Price: Printed Copy A03
Microfiche A01

Distribution Category: Atomic,
Molecular, and Chemical Physics
(UC-411)

ANL-90/20

Argonne National Laboratory
9700 S. Cass Avenue
Argonne, IL 60439

FIXED MASK ASSEMBLY RESEARCH FOR APS INSERTION DEVICES

by
Tuncer M. Kuzay
Materials and Components Technology Division
and
Advanced Photon Source Division

January 1990

Work supported by
U.S. Department of Energy
BES-Materials Sciences

Table of Contents

Tables

Figures

FIXED MASK ASSEMBLY RESEARCH FOR APS INSERTION DEVICES

by Tuncer M. Kuzay

ABSTRACT

The Fixed Mask Assembly (FMA) is the first component to interact with the photon beam. Two sets of a pair of FMA channels, vertically and horizontally disposed, contain the beam rather than define it. They are subject to very large heat fluxes during containment.

In current practice, the FMA channels are made of heavy, seamless copper, have rectangular cross-sections, and are cooled internally with water. Channels are set at grazing angles ranging from 1 to 6 degrees with respect to the beam, depending on the type of insertion device.

APS insertion devices will impose higher heat fluxes on FMAs. Therefore, a need exists to improve the FMA engineering, keeping in mind the current design criteria and philosophy of FMAs.

Preliminary analysis of current heat transfer practice indicates that the major resistance to heat transfer is on the coolant side. Therefore, FMA cooling would benefit from enhanced heat transfer on the coolant side. With this principle in mind, an experimental program has been undertaken to explore the feasibility of using high-performance copper tube configurations which are expected to yield heat transfer coefficients,"h", in single phase flow systems 2 to 5(?) times higher than equivalent plain tubes. In this report, the experimental scope and a preliminary analysis of high-performance copper tube configurations are described.

1. INTRODUCTION

The conceptual design [1] of a typical layout for an undulator front end is shown in Fig. 1.

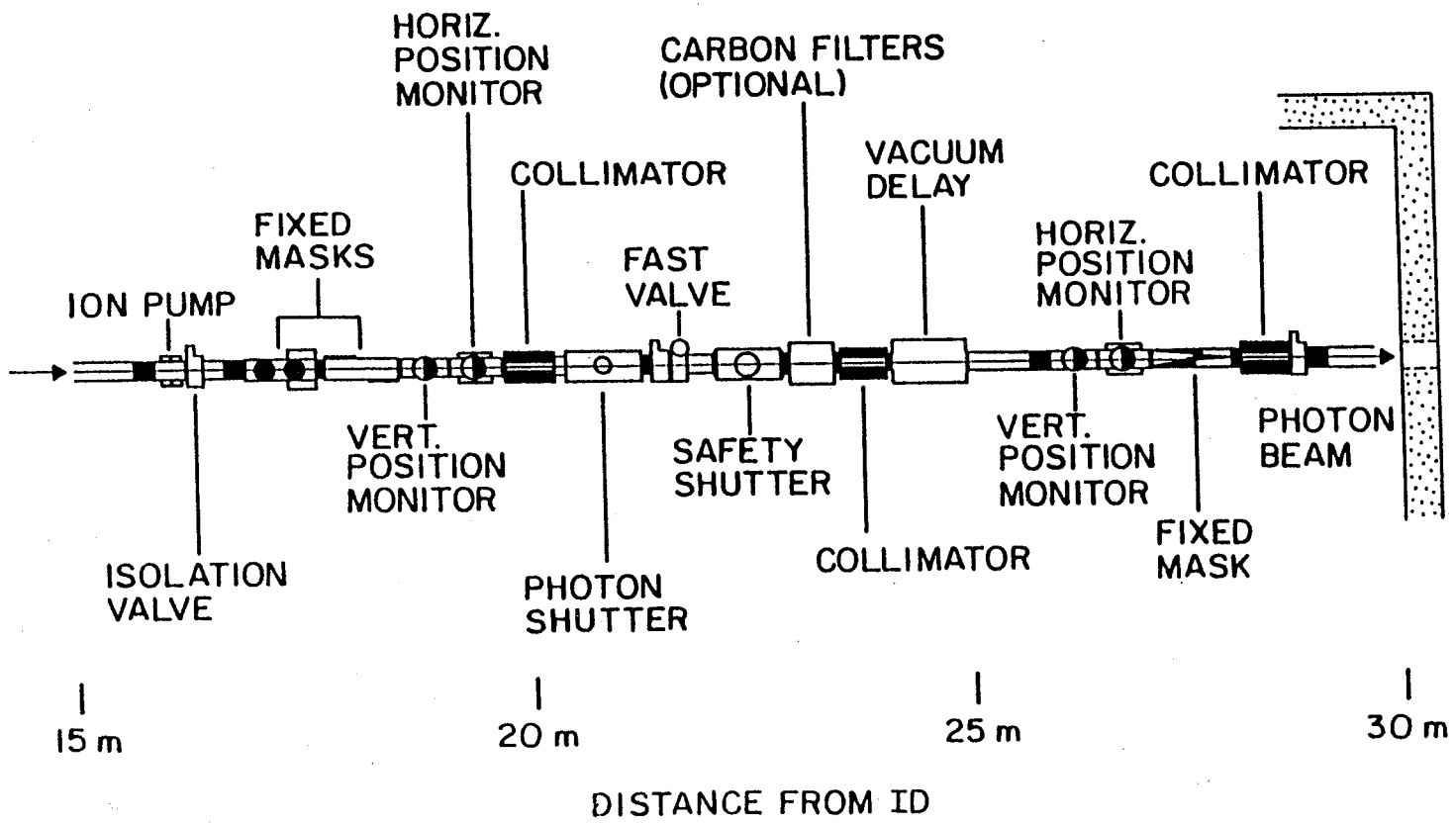

Fig. 1 Typical layout of an undulator front end. The beryllium window is located to the right of the shield wall at approximately 31 m.

The Fixed Mask Assembly (FMA) is the first component to interact with the photon beam. This mask and a second mask downstream define the maximum vertical and horizontal angular excursions of the beam from some predefined center line. The masks are water-cooled copper metal channels and are arranged such that the downstream non-cooled components never intercept any part of the photon beam. In the present design, which is similar to that of the X-17 FMA at the National Synchrotron Light Source (NSLS) [2,3], the horizontal mask consists of two water-cooled copper bars in an open "v" arrangement (see Fig. 2). The vertical mask is made of two sets of bars in closed "v" arrangements above and below the beam. In both cases, the absorbers are set at horizontal grazing incidence to the photon beam. The second set of cooled fixed masks downstream in the front end is similar in design to the first set. In the case of the APS, the masks are designed to contain the beam rather than define it, and must be able to absorb large power densities from part or all of the photon beam.

The masks are positioned at a low to grazing angle to the photon beam to reduce the heat flux levels. Typically these angles vary between one and six degrees, depending on the insertion device used. In Table 1, the current x-ray source parameters for the APS operating at 7 GeV and 100 mA power are presented [1].

A cursory review of the table indicates that Undulator A with a 1.0 cm gap will pose the greatest challenge to the FMA designer. At a distance of 16.5 m from the source, the first set of FMAs will receive a 1400 W/mm^2 heat flux at normal incidence, which is difficult to handle. For a water-cooled copper tube set at a practical six degree angle, the heat flux will be reduced to about 6.7 W/mm^2, and the linear heat flux will be approximately 146.5 W/cm. These numbers should be compared with 4.06 W/mm^2 and 128 W/cm, respectively, for the FMAs on the NSLS X-17 beam line. The design parameters of the X-17 FMAs [3] are listed in Table 2, and the FMA copper channel geometry is shown in Fig. 3.

One-dimensional heat transfer under the beam is characterized by the Biot modulus Bi = ht/k. The 3-D heat transfer effects will be discussed later in this report. Table 3 shows Bi values for FMA operation with Cu and Al metal channels; a metal wall with a thickness of 1/8 in. or 3.2 mm (the typical thickness under the beam area); water coolant; and various values of the heat transfer coefficient, "h". Since for all the practical engineering choices considered in Table 3 the Biot modulus is less than unity, it is obvious that the principal resistance to heat transfer is on the coolant side. Therefore, the simple test of

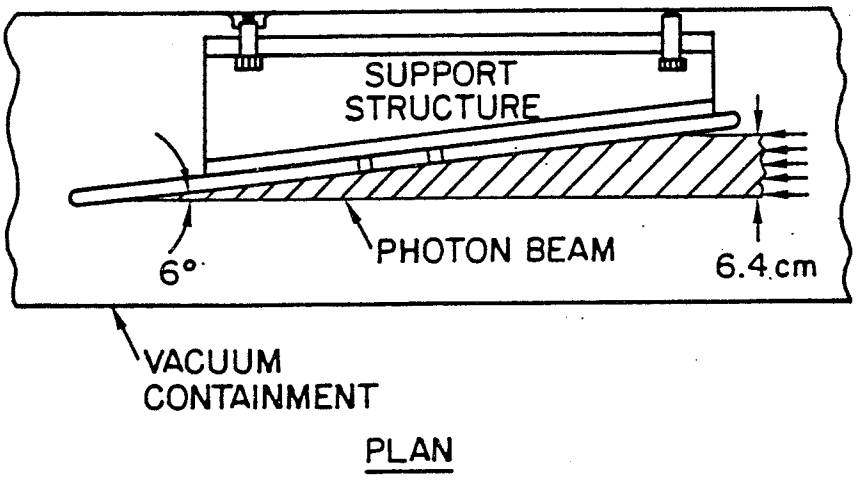

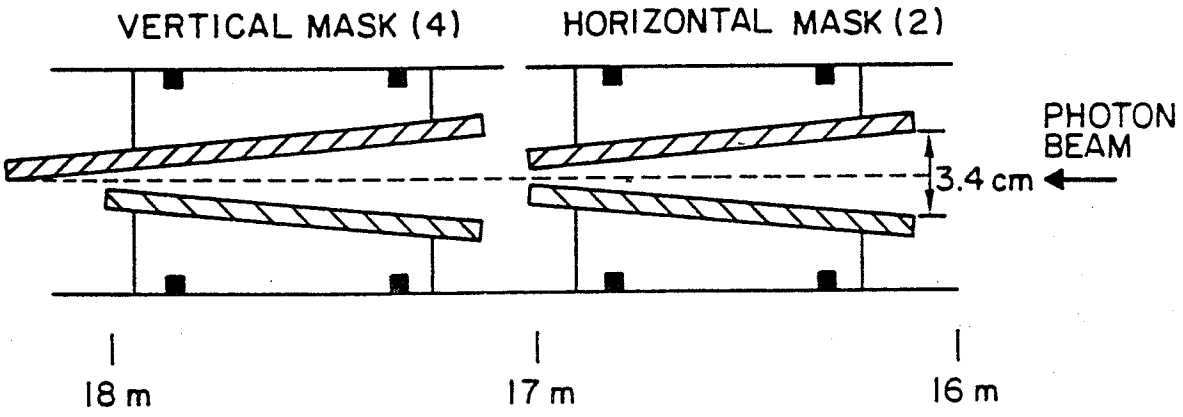

Fig. 2. Partial layout of a fixed vertical and fixed horizontal mask assembly.

TABLE 1. Parameters of x-ray sources for the APS operating at 7 GeV and 100 mA. E is either the critical energy (wiggler or bending magnet) or the undulator first harmonic energy at the magnet gaps indicated. P_K is the peak angular power density; P_A, the linear peak angular power density integrated over the vertical opening angle; P_N, the peak normal power density at 15 m from the source point; and P_T, the total power emitted by the device.

X-ray Source	Period (cm)	Length (m)	E (keV)	B_O (T)	K	P_K (kW/mrad^2)	P_A (kW/mrad)	P_N (W/mm^2)	P_T (kW)
BM	---	---	19.5	0.599	---	0.78	0.086	3.5	0.52
Wiggler A	15	1.5	32.6	1.0	14	26	2.90	116	4.6
Wiggler B	25	5	9.8	0.30	7	15.6	1.74	70	1.4
Undulator A:									
(Gap=2.8 cm)	3.3	5.2	13.5	0.21	0.4	36	4.0	160	0.27
(Gap=1.0 cm)	3.3	5.2	3.5	0.78	2.5	320	35.6	1400	9.8
Undulator B:									
(Gap=1.9 cm)	2.3	5.2	19.3	0.13	0.3	48	5.3	212	0.3
(Gap=1.0 cm)	2.3	5.2	13.0	0.47	1.0	250	28.3	1130	3.6

TABLE 2. NSLS X-17 BEAMLINE ABSORBER DESIGN PARAMETERS

	Horizontal FMAs	Vertical FMAs
Absorber Angle	6 deg	2 deg
Heat Flux (max)	4.06 W/mm^2	1.35 W/mm^2
Linear Heat Load	146.5 W/mm	343 W/mm
Coolant Velocity	6.6 m/s	same
Coolant Rate	0.442 l/s	same
Calculated "h" for 3/8 in. Cu Channel	21000 W/m^2 °C	same
Absorber Length	61 cm	61 cm
Maximum Wall Temperature at Coolant Boundary	66.4 °C	96.7 °C
Maximum Cu Temperature	82.4 °C	111.7 °C

TABLE 3. BIOT MODULUS FOR 1/8-in. THICK WALL AT VARIOUS PRACTICAL "h" VALUES

h		Bi	
BTU/hr ft^2 °F	W/m^2K	Cu	Al
1000	5682	0.04	0.12
3000	17046	0.12	0.36
6000	34091	0.24	0.75

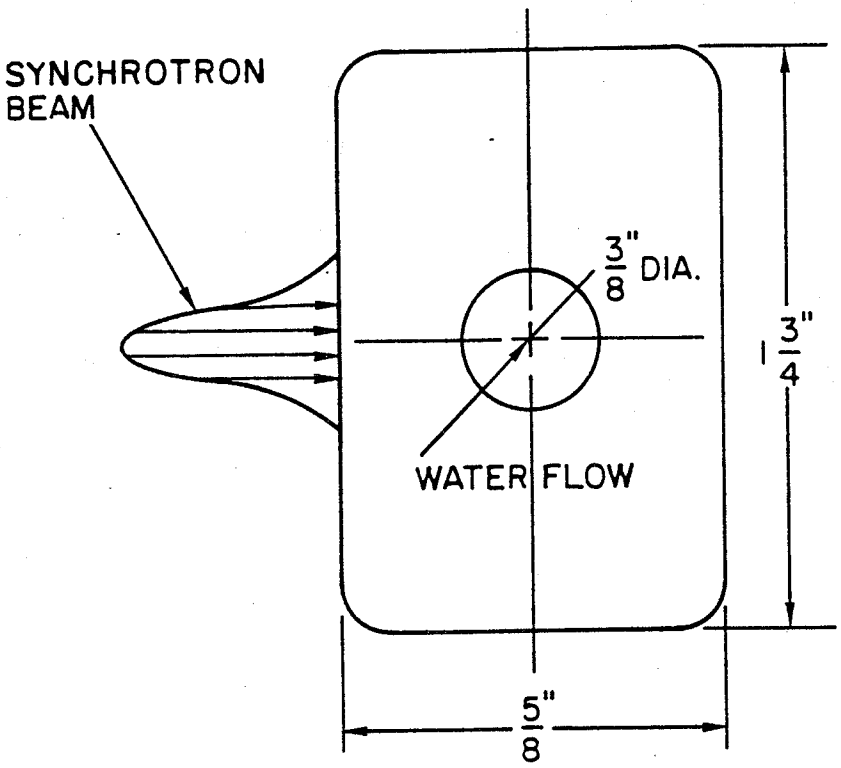

Fig. 3. FMA copper tubing for the NSLS X-17 wiggler.

assessment of heat transfer in an FMA reveals that heat transfer can be improved by employing enhancement techniques on the coolant side.

An examination of Table 4, which shows the expected heat flux levels on an FMA at selected incidence angles, reveals that advanced designs for the APS insertion devices are needed. Compared with the FMA designed for the NLSL Wiggler [2], the APS undulator A poses significant design challenges. A preliminary study [4] of the previous APS FMA designs predicted the data shown in Table 5. The predictions are for an APS undulator, an APS wiggler, and a wiggler of previous design (the NSLS wiggler). Ideally, FMAs should operate safely, reliably, and with ease of control and adjustment. If conventional techniques are followed, it is evident from the data in Table 5 that FMAs for certain APS insertion devices would not meet these requirements. Thus, research was initiated to design and test enhanced heat transfer tubes suitable for the FMA in the APS.

2. LITERATURE SEARCH

The literature on enhanced heat transfer in FMAs is extensive. Confining the FMA design to simple geometries and enhancement methods, the use of inner-surface-roughness features can yield 2-3-fold increases over plain tubes [5]. The new high performance tubes available from a few companies [e.g. 6] yield enhancement levels of three-fold over plain tubes (Fig. 4).

Incorporation of such high performance tubes in the FMA design may result in attainment of any of the following design goals:

- tolerance of higher heat flux levels for the same wall temperatures
- reduction of coolant velocity/flow rate for the same performance
- reduction of pressure drop for the same performance
- increase in the angle of incidence of the beam on the FMA tube
- decrease in the FMA tube length.

To illustrate, for an enhancement level of 2.5-fold, the coolant velocity can be reduced, on average, by a factor of $(2.5)^{0.8} \cong 2.1$ for the same heat transfer coefficient, "h". Conversely, "h" can be increased by a factor of ~2.1 at the same

TABLE 4 PARAMETERS OF SELECTED X-RAY SOURCES FOR THE APS OPERATING AT 7 GeV AND 100 mA AND SAMPLE PEAK HEAT FLUXES AT ASSUMED INCIDENCE ON THE FMA SURFACE

Insertion Device	Normal Beam Opening at Source σ_H (mrad)	$\pm \sigma_V$ (mrad)	Beam Footprint at 16.5 m σ'_H (mm)	σ'_V (mm)	P_N at 16.5 m (W/mm^2)	Assumed FMA Angle (deg)	Peak Flux P_k at Incidence Angle (W/mm^2)
Undulator A	0.182	0.044	3.0	0.73	1157	1	10.1
Wiggler B	0.511	0.044	8.43	0.73	58	6	3.04
Wiggler A	1.022	0.044	16.7	0.73	96	2	1.68

TABLE 5. PREDICTED FMA TEMPERATURES FOR APS INSERTION DEVICES [4]

	APS Undulator A	APS Wiggler B	APS Wiggler B	NSLS Wiggler [3]
Peak Power (W/mm^2)	19.2	11.5	3.8	4.06
Included Angle (degree)	1	6	2	6
Beam Footprint (cm x cm)	0.141 x 41.2	0.141 x 34.6	0.141 x 103	
Coolant Velocity (fps)	20	20	20	20
T_{max} - surface (°C)	212	138	64.7	78
T_{max} - wall (°C)	127.5	88	48.1	62
T_{bulk} - coolant (°C) at Entrance	26.7	26.7	26.7	25

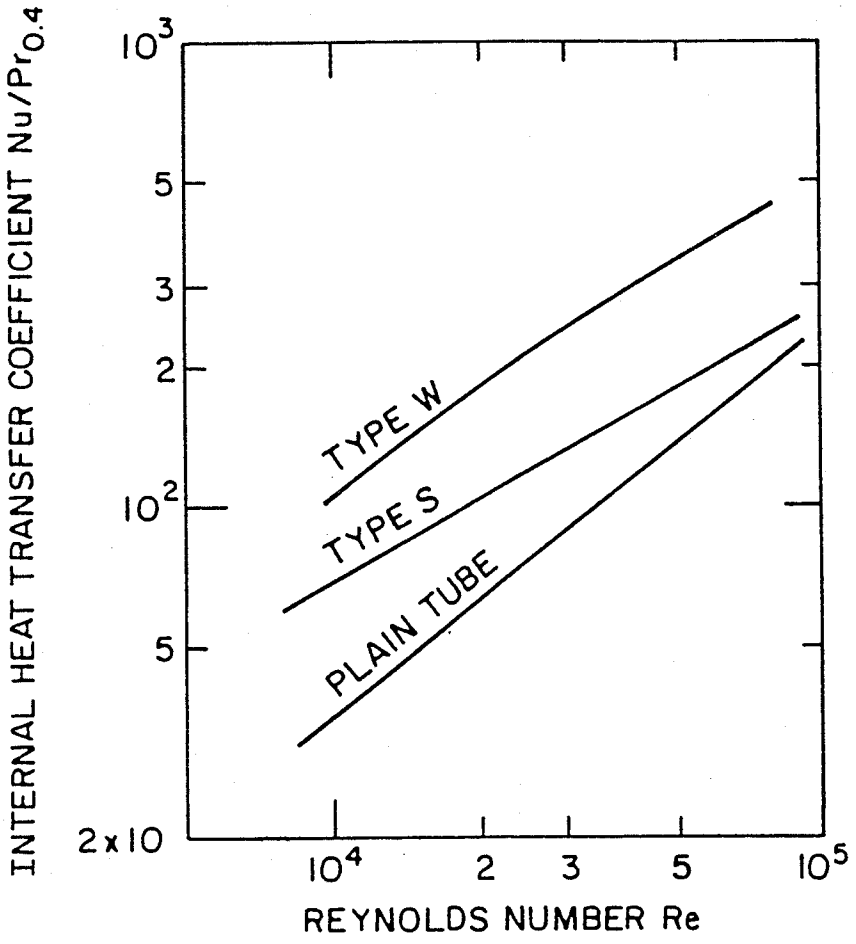

Fig. 4. Internal heat transfer coefficient of Hitachi Thermofin-SP tube [6].

velocity or flow rate. Attainment of a higher "h" is beneficial for the current practice of FMA engineering as the earlier, simple analysis indicated (Table 3).

Also, as noted previously (Table 4), the APS undulators and certain wigglers impose much larger heat flux levels compared to the reference NSLS Wiggler on the X-17 beam line. Thus, tubes that provide enhanced heat transfer will be particularly useful at the APS. For the NSLS X-17, the design "h" is 17,000 W/m^2K attained at a coolant velocity of 20 fps. Table 3 indicates that by using a copper tube, one could increase "h" up to 8 fold (Bi~1.0), resulting in better heat transfer in convection. But, because the coolant velocity is already 20 fps and with an accompanying large pressure drop, increased performance using the same type of tube is unlikely. Therefore, the use of tubes with enhanced heat transfer provides a significant design improvement which will be particularly critical for the APS insertion devices. With an aluminum tube, on the other hand, up to a 3-fold enhancement in "h" is possible.

With respect to the copper tube designs, other practical enhancement methods which will yield on the order of 5-fold or higher increases in "h" have been reported. Short of using liquid metals as the coolant, the meager amount of information in the open literature [7,8] indicates that tubes filled with conductive metallic matrices (metal foams, sponges, or porous plugs) yield very high levels of enhancement in heat transfer. These studies report phenomenal [O(10) or so] increases in heat transfer with metallic porous fillers in a single-phase flow system, and even larger increases in a two-phase flow system. Unfortunately, the data in these two key studies (as well as about a dozen other related Russian works) are not well presented, the translations are inaccurate, and the data plots are not reliable. Therefore, we propose a simple experimental investigation to examine the claims made in these works.

3. EXPERIMENTAL PROGRAM

Two sets of tube configurations were chosen for the experimental program. The first set consists of two similar tubes developed in Japan and Germany, respectively. These copper tubes have interrupted turbulator elements on their internal walls set in a helical pattern. The tubes were supplied to ANL, courtesy of their respective manufacturers:

i. Hitachi Cable America, Inc. of White Plains, NY, and
ii. Wieland-Werke AG of Ulm, West Germany.

The expected performance of these tubes is exemplified by the performance curves supplied in the Hitachi Cable catalog, particularly that of the type "W", tube (Fig. 4). An examination of this figure shows that a high performance tube will exhibit better than a 2.0-fold increase in "h" compared to a plain tube of similar size. The Wieland-Werke tube is expected to perform similarly.

The second category of tubes consists of rectangular heavy-wall copper tubes as shown in Fig. 5. Four such tubes are being prepared for testing. Each specimen is approximately 61 cm (26 in.) long; one is entirely plain and the other three are filled with and brazed to a copper mesh. The filler porosity is either 70, 80, or 90 percent . The tubes will be heated on all four sides using self-adhesive thin film heaters (total heat load is about 2 kW), as shown in Fig. 5. The amount of heat transfer at various Reynolds numbers will be measured in these tubes using water as the coolant. The difference in the experimentally measured "h" between the plain and the filled tubes will determine the level of enhancement achievable at various practical porosities, and correlations will be generated. Although the heat transfer performance of the Hitachi Cable/Wieland type high performance tubes is not expected to be as high as the "anticipated performance" of the copper filled tubes, the former already afford a significant design improvement over current practices. Thus, regardless of the outcome of the research on copper-mesh filled tubes, use of enhanced-performance copper tubes will improve the APS FMA designs. At the APS, where the heat loads and heat fluxes will be higher than at the NSLS, the importance of enhanced-performance tubes in the design of the APS FMAs cannot be overemphasized. To be sure, the question is not whether we should use enhanced tubes, but rather how we can get greater heat transfer enhancement in the FMA tubes while keeping the other safety/operational criteria the same.

4. PREDICTED BENEFITS FROM ENHANCED HEAT TRANSFER TUBES

Without a specific in-depth analysis (which will be conducted subsequent to the experimental program), one can make an educated guess about the benefits to be derived from using an enhanced-heat-transfer tube in the FMA design.

The fundamental heat transfer problem of a plate subject to a centrally located X-ray beam in 2-D is solved in Appendix A. The plate is wider than the beam (normalized beam width is 2α, and normalized plate width is 2β). The beam

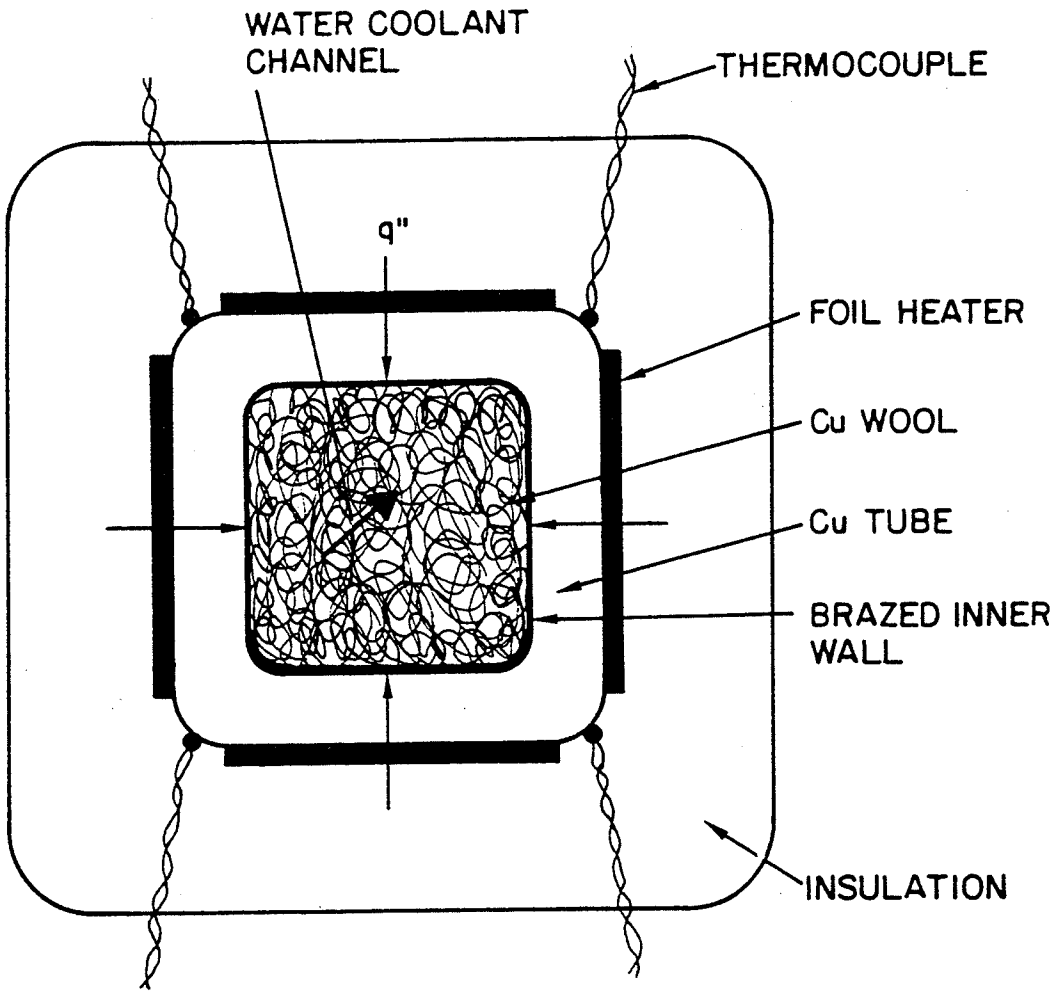

Fig. 5. Copper wool filled rectangular heavy-wall copper tubing.

imposes a uniform surface heat flux on the convectively cooled plate. This solution can be contrasted with the problem presented in reference [9], which was in 3-D and involved a finite square beam footprint incident on a convectively cooled finite target. The formulation and solution presented in Appendix A are more representative of the generalized FMA heat transfer problems in which the beam footprint is long because of the grazing angle at which the absorber channel is set with respect to the beam.

Selected results from the analysis presented in Appendix A are shown in Fig. 6. This figure depicts the normalized maximum center temperature $\theta_{max}(0,0)$ against the Biot number as a function of β/α ratio (shown as b/a in Fig. 6). The results in the figure are all for a practical case of $\beta = 6.0$ (note that, for the NSLS FMA [3], the nominal β is also 6) i.e., $b/t = \frac{1.5"}{2} \times \frac{1}{0.125}$.

In Fig. 6, the $\theta_{max}(0.0)$ levels off approximately after $Bi \cong 1.0$ for all cases. For the practical engineering design range of $0.1 < Bi < 1.0$, there is a significant drop in $\theta_{max}(0.0)$ with increasing Bi toward 1.0. The smaller the β/α ratio (increasing absorber channel width relative to the X-ray beam width), the larger the reduction in $\theta_{max}(0.0)$, as is expected on physical grounds. In the extreme case of an absorber in which $\beta/\alpha = 1.0$, the highest θ_{max} results (which is independent of x or ξ). This special but trivial case is marked with circle symbols in Fig. 6.

The reduction of the maximum temperature on the absorber surface derived by increasing the coolant side heat transfer coefficient toward $Bi \sim 1.0$ is evident from Fig. 6. This theoretical prediction will be tested using the enhanced heat transfer tubes described in this report.

5. CONCLUSIONS

This report details the present design approaches for the FMA for the APS. It is shown that FMAs will benefit from heat transfer enhancement on the coolant side. An experimental and analytical program has been initiated to investigate two kinds of enhanced-heat-transfer tubes to be used in the FMA. One kind of tube is offered by industry and uses internal surface modifications (knurled surface interruptions in a spiraling configuration) to achieve enhancement. The level of heat transfer augmentation in a single-phase flow system using such an

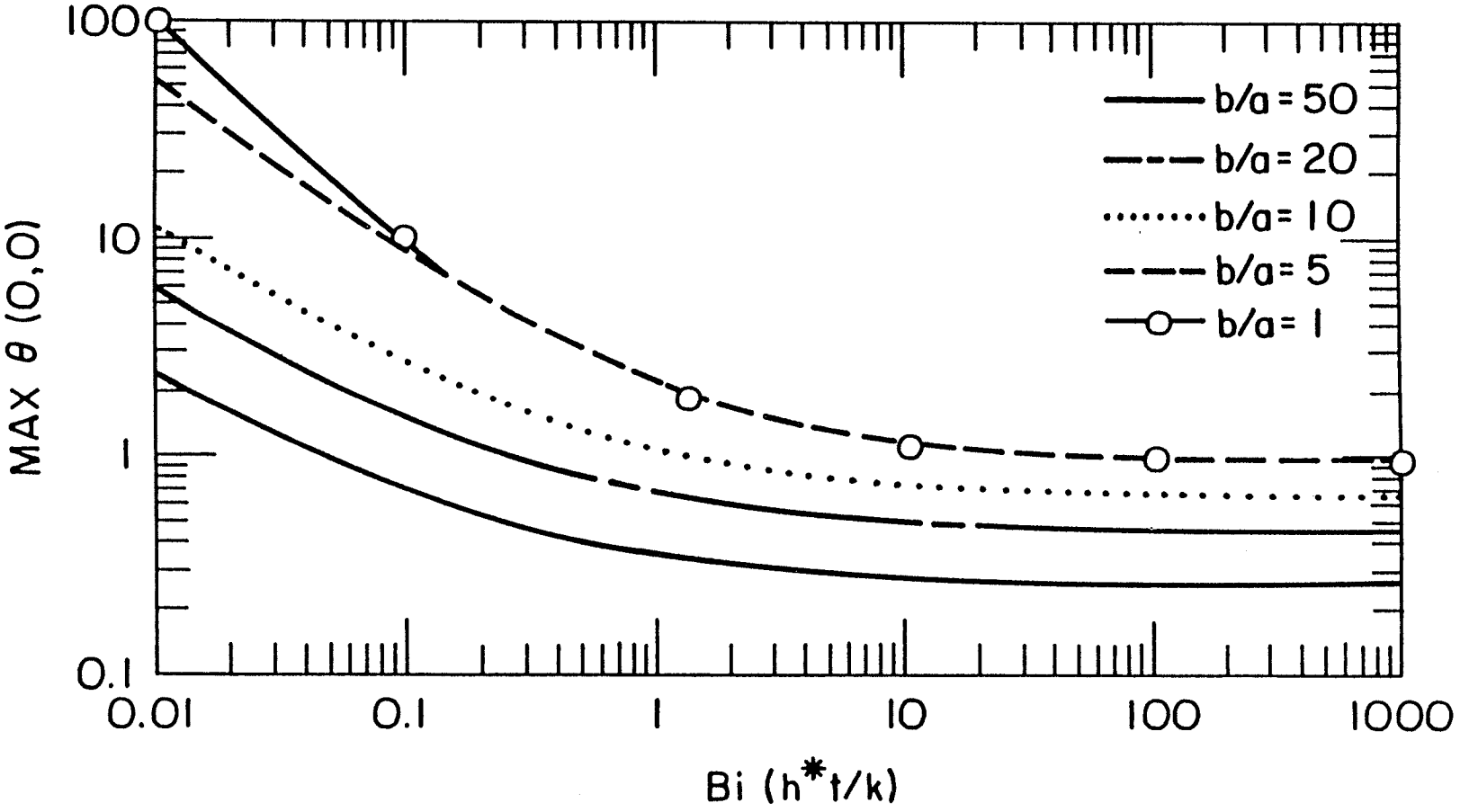

Fig. 6 Maximum centerline temperature, $q_{max}(0,0)$, vs Biot modulus for different absorber width to beam width ratios.

enhanced tube is expected to be 2-3-fold. The second kind of tube is being developed in-house, and consists of a copper tube filled to various porosities with a copper matrix (sponge, foam) brazed to its internal walls. Using this type of tube, the expected level of heat transfer enhancement is currently unknown, but existing sources, if reliable, cite very large enhancement levels, O(5-10). The experiments described in this report will determine the level of heat transfer enhancement that can be expected using such tubes.

It is expected that the use of enhanced-heat-transfer tubes in the FMA design for the APS insertion devices should not pose a formidable challenge to the designer.

The present study precludes other heat transfer options such as:

- Low-Z covered FMAs (with Be, for example)
- Liquid metal cooling
- High boiling point special heat transfer fluids.

6. ACKNOWLEDGEMENTS:

The solution suggested by Mun Soo Choi of APS to the problem formulation presented in Appendix A is greatly appreciated. Careful typing by RoseMary Barrera is also appreciated.

7. REFERENCES

[1] Viccaro, P. J., "A Front End Design for the Advanced Photon Source," APS, LS-108 (April 1988).

[2] Thomlinson, W., "NSLS Superconducting Wiggler Beam Line (X17) Conceptual Design Report," Brookhaven National Laboratory Informal Report (1984).

[3] Ulc, S. and Sharma, S., "A Thermal Absorber for High Power Density Photon Beams," Nucl. Instr. and Methods, **A246**, 423 (1986).

[4] Kuzay, T. M., and Rezaian, R., Argonne National Laboratory, unpublished information (1987).

[5] Bergles, A. E., "Techniques to Augment Heat Transfer," Handbook of Heat Transfer Applications, eds. W. M. Rohsenow, et al., (McGraw Hill, New York, 1985).

[6] Hitachi High-Performance Heat-Transfer Tubes, Cat. No. EA-500B, 1988.

[7] Maiorov, V. A., Polyaev, V. M., Vasil'ev, L. L., and Kiselev, A. I., "Intensification of Convective Heat Exchange in Channels with Porous High-Thermal-Conductivity Filler. Heat Exchange with Local Thermal Equilibrium Inside the Permeable Matrix," Inzhenerno-Fizicheskis Zhurnal, **47**, (1), 13-24 (July 1984).

[8] Apollonov, V. V., et al., " Thermophysical Principles of Cooled Laser Optics Based on New-Type Penetrable Structures," Experimental Heat Transfer, Fluid Mechanics, Thermodynamics, eds. R. K. Shah, et al., (Elsevier Science Publishing Co., New York, 1988), pp. 882-92.

[9] Kuzay, T. M., "Cooling Augmentation in X-ray Optics," Presented at the Workshop on High Heat Load X-ray Optics, Argonne National Laboratory, Aug. 3-5, 1989.

8. APPENDIX

The steady-state, two dimensional problem of a long x-ray beam incident on an absorber wider than the beam width is sketched in Fig. A.1.

This problem is amenable to a closed-form solution. The formulation and solution are presented below:

$$\frac{\partial^2 T}{\partial x^2} + \frac{\partial^2 T}{\partial y^2} = 0, \qquad (1)$$

subject to the following boundary conditions:

$$-k \frac{\partial T}{\partial y}(x,0) = q \qquad 0 < x \leq a \qquad (2)$$

$$-k \frac{\partial T}{\partial y}(x,0) = 0 \qquad a < x \leq b$$

$$-k \frac{\partial T}{\partial y}(x,t) = h\,(T - T\infty) \qquad (3)$$

$$\frac{\partial T}{\partial x}(0,y) = \frac{\partial T}{\partial x}(b,y) = 0 \qquad (4)$$

Equations (1) and (4) can be non-dimensionalized by defining the following normalization terms:

$$\alpha = \frac{\alpha}{t}$$

$$p = \frac{b}{t}$$

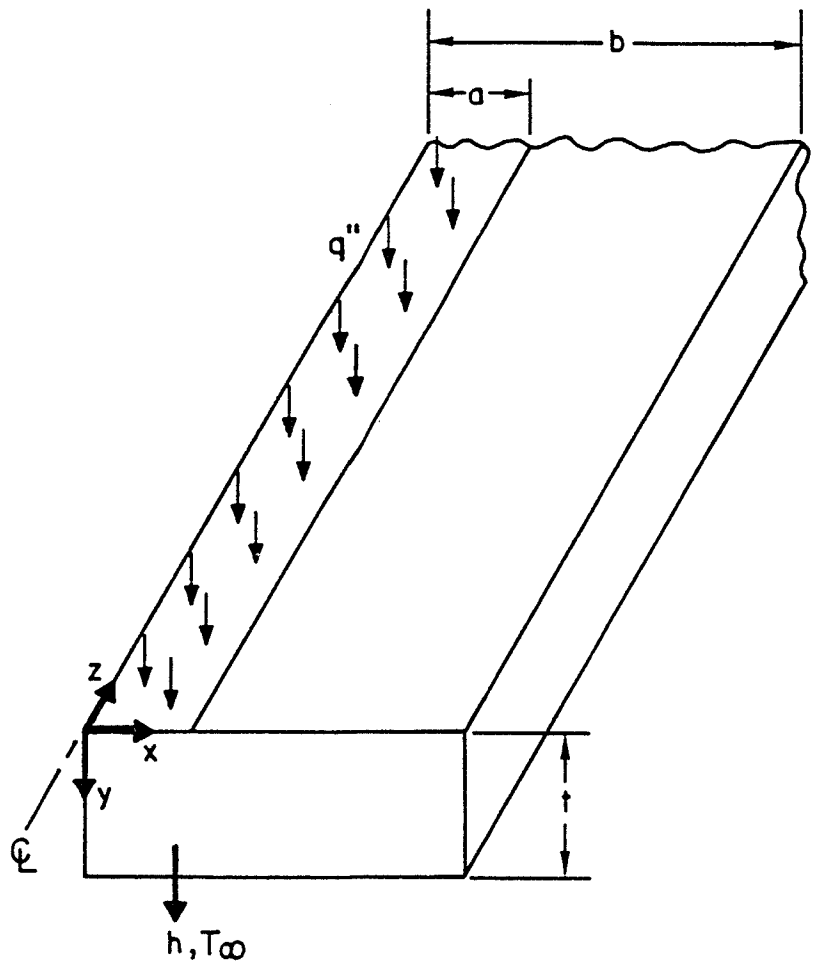

Fig. A.1. Half absorber plate geometry of the problem formulation.

$$\xi = \frac{x}{t}$$

$$\eta = \frac{y}{t}$$

$$\theta = \frac{T - T\infty}{q \frac{t}{k}}$$

$$Bi = \frac{ht}{k} \tag{5}$$

Then,

$$\frac{\partial^2\theta}{\partial\xi^2} + \frac{\partial^2\theta}{\partial\eta^2} = 0 \tag{6}$$

subject to the boundary conditions

$$+\frac{\partial\theta}{\partial\eta}(\xi,0) = -1 \qquad 0<\xi\leq\alpha$$

$$f(\xi)$$

$$\frac{\partial\theta}{\partial\eta}(\xi,0) = 0 \qquad 0<\xi\leq\beta \tag{7}$$

$$-\frac{\partial\theta}{\partial\eta}(\xi,1) = Bi\ \theta \tag{8}$$

$$\frac{\partial\theta(0,\eta)}{\partial\xi} = \frac{\partial\theta(\beta,\eta)}{\partial\xi} = 0 \tag{9}$$

The following solution is obtained by using separation of variables [the problem is non-homogenous only for boundary condition (7)]:

$$\theta(\xi,\eta) = X(\xi)\ Y(\eta) \tag{10}$$

From eqn. (6),

$$\frac{X''}{X} = -\frac{Y''}{Y} = \lambda_m^2 \quad \text{with solutions}$$

$$X(\xi) = C_1 \cos(\lambda_m \xi) + C_2 \sin(\lambda_m \xi) \tag{11}$$

$$Y(\eta) = C_3 e^{-\lambda_m \eta} + C_4 e^{\lambda_m \eta} \tag{12}$$

Using boundary condition (9) and from (10), for

i) $\lambda_m \neq 0$

$$X(\xi) = C_1 \cos(\lambda_m \xi) \ , \ \lambda_m = \frac{m\pi}{\beta} \qquad m=1,2,3,.-0 \tag{13}$$

$$Y(\eta) = C_4 e^{-\lambda_m \eta} \left[1 + e^{2\lambda_m (\eta-1)} \frac{\lambda_m - Bi}{\lambda_m + Bi} \right] \tag{14}$$

ii) $\lambda_m = 0$

from the general solutions

$$Xo = a\xi + b$$

$$Yo = c\eta + d \tag{15}$$

$$Xo = b$$

$$Yo = c \left[\eta - 1 - \frac{1}{Bi} \right] \tag{16}$$

Then, with no loss of generality for linear equations

$$\theta(\xi, \eta) = \theta o + \sum_{m=1}^{\infty} \theta m \tag{17}$$

the solution of (6) is found to be

$$\theta_m = C_o\left[\eta - 1 - \frac{1}{Bi}\right] + \sum_{m=1}^{\infty} C_m \cos(\lambda_m \xi) e^{-\lambda_m \eta x}$$

$$\left[1 + e^{+2\lambda_m (\eta - 1)} \frac{\lambda_m - Bi}{\lambda_m + Bi}\right] \qquad (18)$$

C_o and C_m's are determined by using the orthogonality condition and applying the unused boundary condition (7) as follows:

At $\eta = 0$

$$f(\xi) = \frac{\partial \theta_m}{\partial \eta} = C_o + \sum_{m=1}^{\infty} \lambda_m C_m \cos(\lambda_m \xi) \left[-1 + e^{-1\lambda_m} \frac{\lambda_m - Bi}{\lambda_m + Bi}\right] \qquad (19)$$

where $f(\xi) = -1 \qquad 0 < \xi \leq \alpha$

$f(\xi) = 0 \qquad \alpha < \xi \leq \beta \qquad (20)$

Then,

$$C_o = -\frac{\alpha}{\beta}$$

$$C_m = \frac{-\int_o^{\alpha} \cos(\lambda_m \xi)\, d\xi}{\lambda_m \left[-1 + e^{-2\lambda_m} \frac{\lambda_m - Bi}{\lambda_m + Bi}\right] \int_o^{\beta} \cos^2(\lambda_m \xi)\, d\xi} \qquad (21)$$

or,

$$C_m = \frac{2 \sin(\lambda_m \alpha)}{\lambda_m^2 \beta \left[1 - e^{-2\lambda_m} \frac{\lambda_m - Bi}{\lambda_m + Bi}\right]} \tag{22}$$

which completes the full solution as follows:

$$\theta_m = C_o \left[\eta - 1 - \frac{1}{Bi}\right] + \sum_{m=1}^{\infty} C_m \cos(\lambda_m \xi)\ e^{1\lambda_m \eta}\ x$$

$$\left[1 + e^{+2\lambda_m(\eta - 1)} \frac{\lambda_m - Bi}{\lambda_m + Bi}\right] \tag{23}$$

where

$$C_o = -\frac{\alpha}{\beta}$$

$$C_m = \frac{2 \sin(\lambda_m \alpha)}{\lambda_m^2 \beta \left[1 - e^{-2\lambda_m} \frac{\lambda_m - Bi}{\lambda_m + Bi}\right]} \tag{24}$$

Special Cases

i) $\alpha = \beta$ $\qquad \frac{\alpha}{\beta} = 1$

In this case, from eqns. (23) and (24),

$$\theta(\xi, \eta) = \left[1 + \frac{1}{Bi} - \eta\right],$$

which is the steady-state solution of a trivial case. The maximum temperature is on the $\eta = 0$ surface and the minimum is on the $\eta = 1$ surface, which are given for their well known magnitudes respectively.

$$\theta_{max}(\xi, 0) = 1 + \frac{1}{Bi}$$

$$\theta_{min}\ (\xi,1) = \frac{1}{Bi} \qquad (25)$$

ii) θ_{max} for the general case is given at θ (0,0) as follows:

$$\theta_{max}\ (0,0) = \frac{\alpha}{\rho}\left(1 + \frac{1}{Bi}\right) + \sum_{m=1}^{\infty} \frac{2 \sin\left(m\pi\frac{\alpha}{\beta}\right)}{\frac{\pi^2 m^2}{\beta}} \frac{1 + L_m}{1 - L_m} \qquad (26)$$

where $$L_m = e^{-2\lambda_m} \frac{\lambda_m - Bi}{\lambda_m + Bi} \qquad (27)$$

ii) In the general case, the maximum temperatures occur at the top surface, and have a distribution as follows:

$$\theta_{max}\ (\xi,o) = \frac{\alpha}{\beta}\left(1+\frac{1}{Bi}\right) + \sum_{m=1}^{\infty} \frac{2 \cos\left(\lambda_m \xi\right) \sin\left(\lambda_m \alpha\right)}{\beta \lambda_m^2} \frac{1 + L_m}{1 - L_m} \qquad (28)$$

Distribution for ANL-90/20

Internal:

Y. Cho
R. Fenner (2)
R. H. Huebner
D. E. Kasza
T. M. Kuzay (43)
D. M. Mills
D. E. Moncton
W. J. Shack
G. K. Shenoy
R. A. Valentin
P. J. Viccaro
R. W. Weeks
ANL Patent Dept
ANL Contract File
APS Document Control Center (2)
TIS Files (3)

External:

DOE-TIC, for distribution per UC-411 (35)
DOE Chicago Operations Office:
    Manager
ANL Libraries (2)